Electronic Supplementary Material (ESI) for Journal of Materials Chemistry A.

Supporting Information

Low powered, tunable and ultra-light Aerographite sensor for climate relevant gas monitoring

O. Lupan,[a,b,†] V. Postica,[b] M. Mecklenburg,[c] K. Schulte,[c,‡] Y. K. Mishra,[a] B. Fiedler[c,‡] and R. Adelung[a,‡]

[a.] *Functional Nanomaterials, Faculty of Engineering, Institute for Materials Science, Christian-Albrechts Universität zu Kiel, Kaiserstr. 2, D-24143, Kiel, Germany.*

[b.] *Department of Microelectronics and Biomedical Engineering, Technical University of Moldova, 168 Stefan cel Mare Av., MD-2004 Chisinau, Republic of Moldova.*

[c.] *Institute of Polymers and Composites, Hamburg University of Technology, Denickestr. 15, D- 21073 Hamburg, Germany.*

†Corresponding author: e-mail ollu@tf.uni-kiel.de oleg.lupan@mib.utm.md lupanoleg@yahoo.com
‡ e-mail ra@tf.uni-kiel.de ra@tf.uni-kiel.de. , fiedler@tuhh.de , schulte@tuhh.de

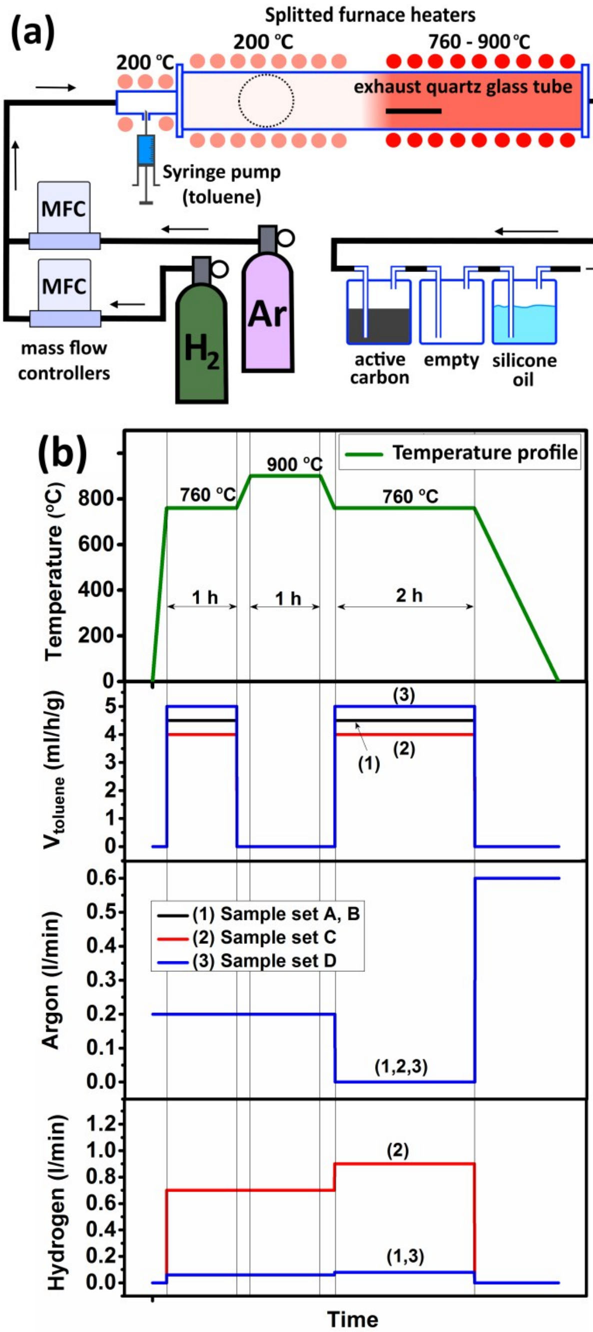

Figure S1. (a) Schematic representation of the nanotechnological system for synthesis of 3-D-microtube network samples from 2-D graphene/nanographite with nanoscopic wall thicknesses called Aerographite. (b) The temperature profile of furnace and all times and phases of variable carbon feeding and variable gas concentrations for synthesis of different types of Aerographite samples (A, B, C and D).

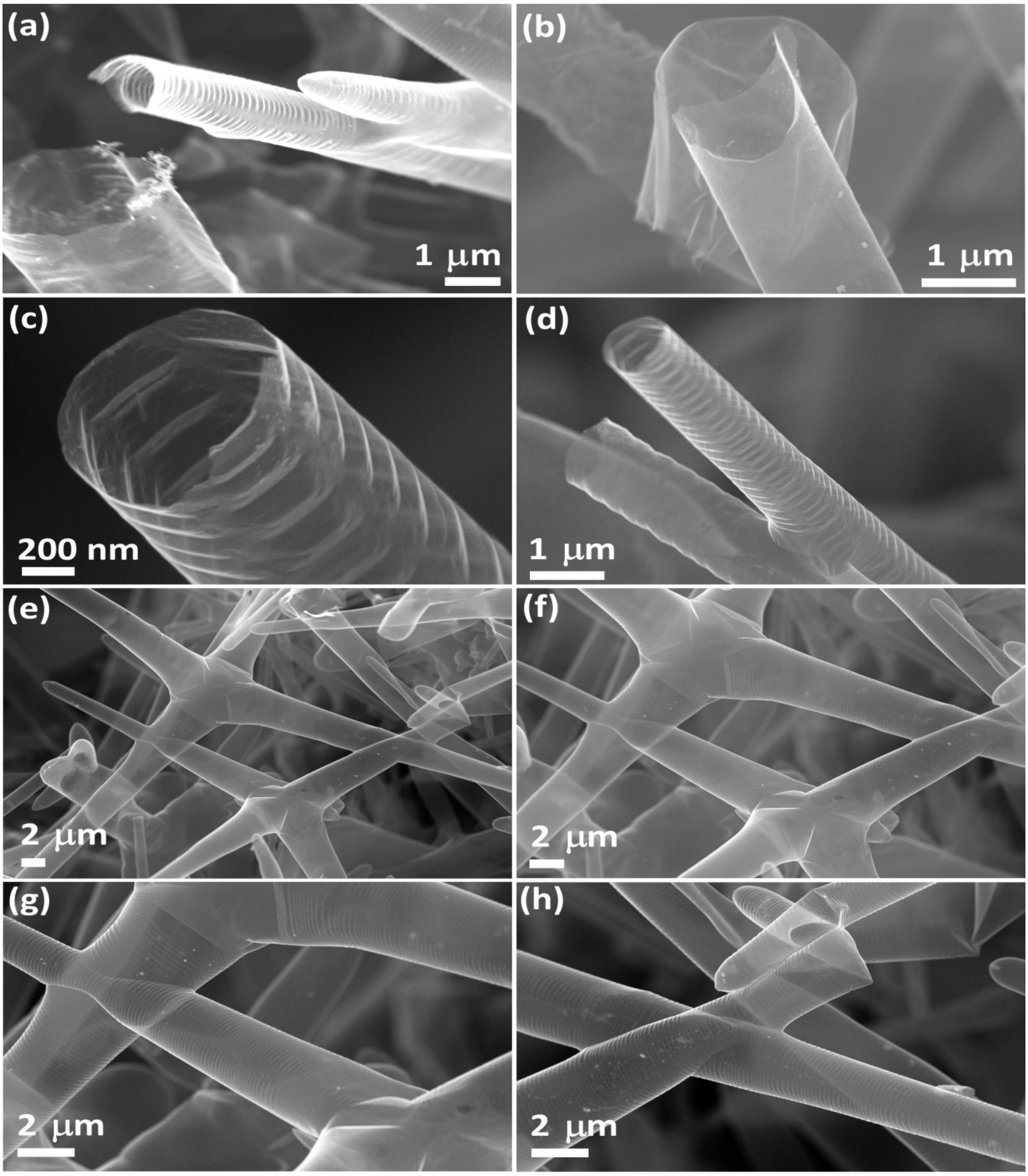

Figure S2. SEM images of Aerographite Sample set A: (a) top view of graphitic tubular tetrapod arms with opened and closed ends; (b) a bent tubular graphitic structure, demonstrating flexibility of the material; (c) a single graphitic tubular tetrapod arm with open end; (d) interpenetrated hollow nanographite tetrapod arms; (e-h) interpenetrated hollow nanographite tetrapods showing excellent connections between graphitic tubular tetrapods, as well as perfect replication of ZnO sacrificial template used for its synthesis.

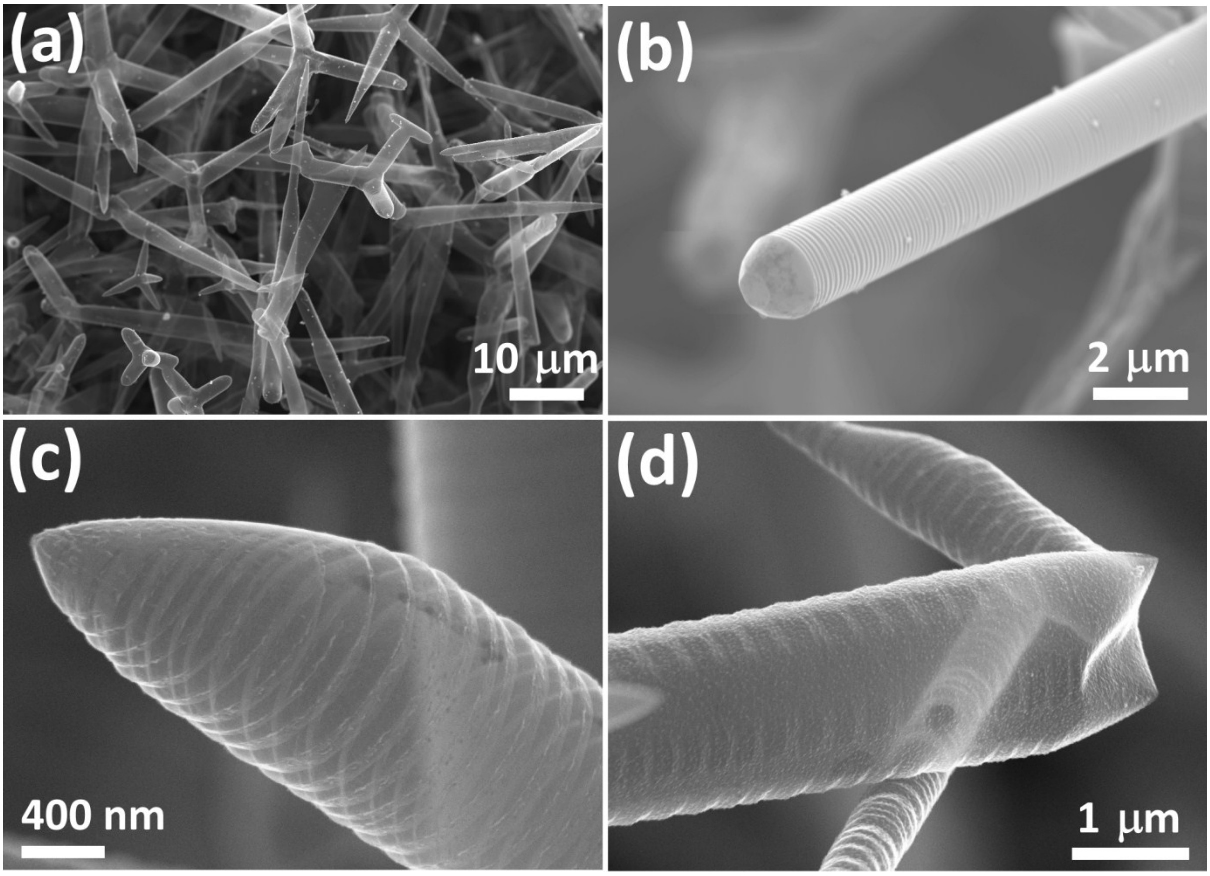

Figure S3. SEM images of Aerographite Sample set A tubular structures with nanoscopic graphitic walls of: (a-c) Aerographite from different regions of the sample from overall view to zoomed tetrapod arm; (d) a bent tubular graphitic structure, demonstrating flexibility of the material.

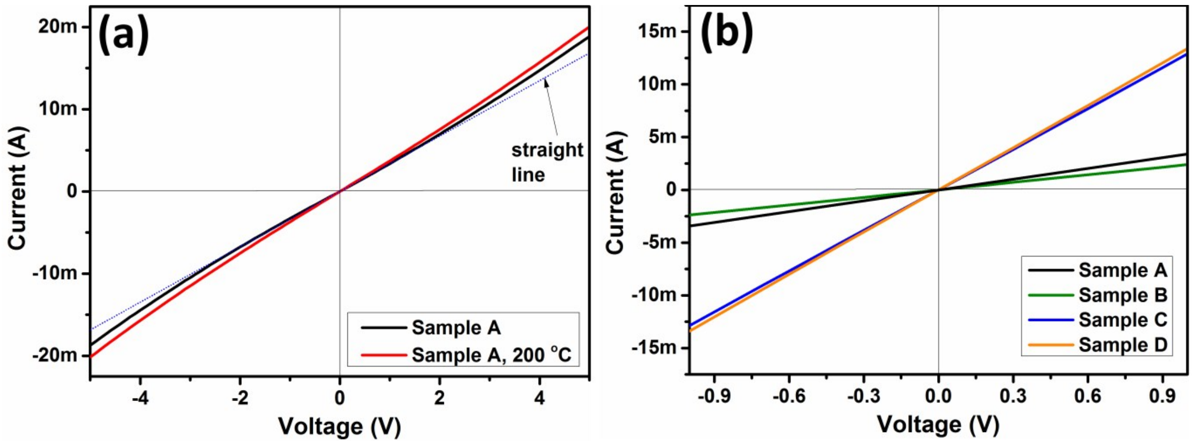

Figure S4. (a) Current – voltage characteristics of the sensor device based on Aerographite Sample set *A* at room temperature and at 200 °C. Straight dotted line is drawn for guiding viewer's eye only. (b) Current – voltage characteristics of the sensor devices based on Aerographite Sample sets *A*, *B*, *C* and *D* at room temperature.

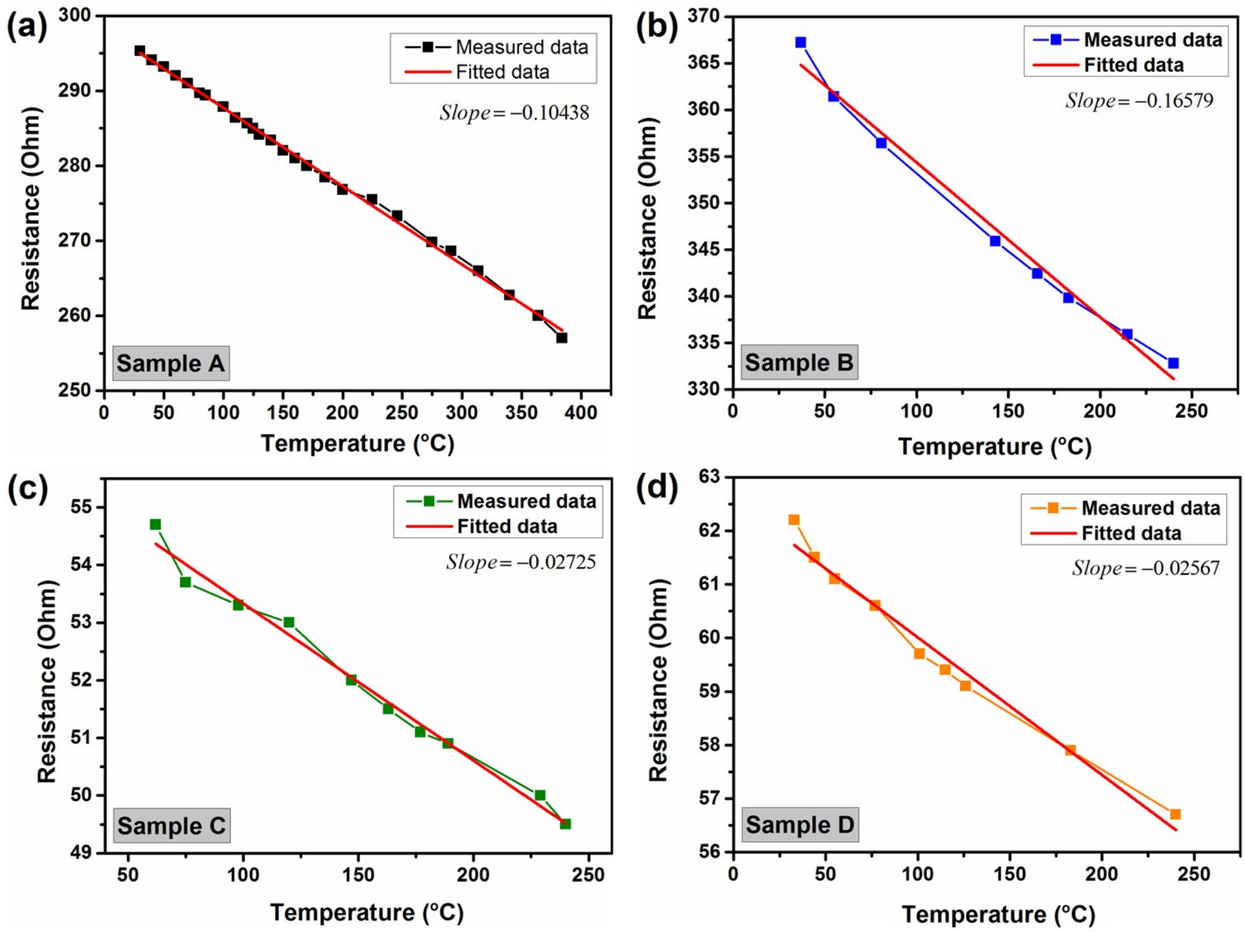

Figure S5. Electrical resistance of the sensor structures based on Sample sets: (a) *A*; (b) *B*; (c) *C*; and (d) *D* as a function of temperature (using an external heater).

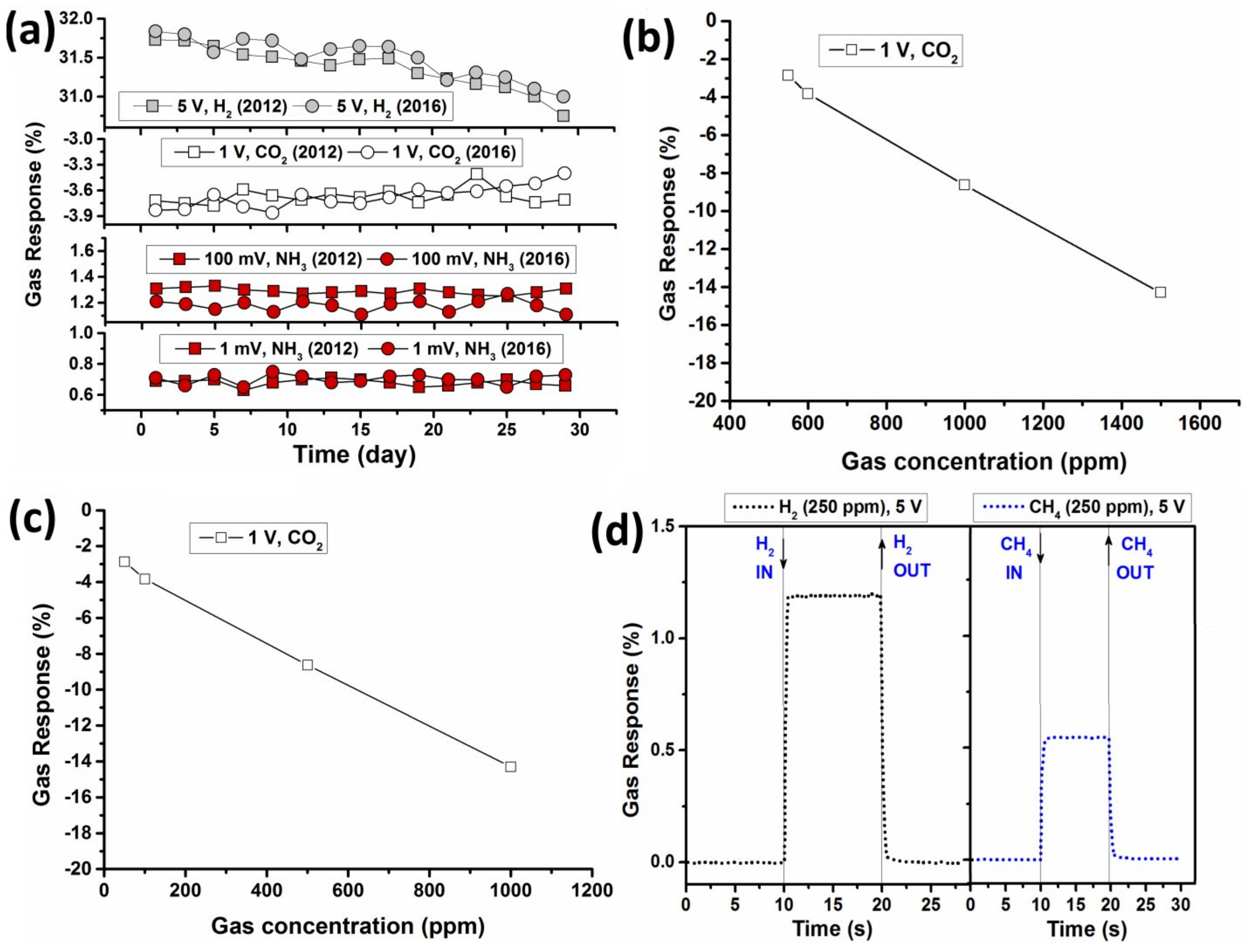

Figure S6. (a) Long time gas response for sensor devices based on Sample sets *A* synthesized in 2012 and 2016 (for comparison reasons) at different applied bias voltages: (1) 1 mV to NH_3; (2) 100 mV to NH_3; (3) 1 V to CO_2; and (4) 5 V to H_2 gas. Gas response for sensor devices based on Samples set *A* at applied bias voltage: (b) 5 V versus concentration of H_2 gas; and (c) 1 V versus concentration of CO_2 gas. (d) Dynamic gas response to 250 ppm of H_2 and CH_4 gas at room temperature and 5 V applied bias.

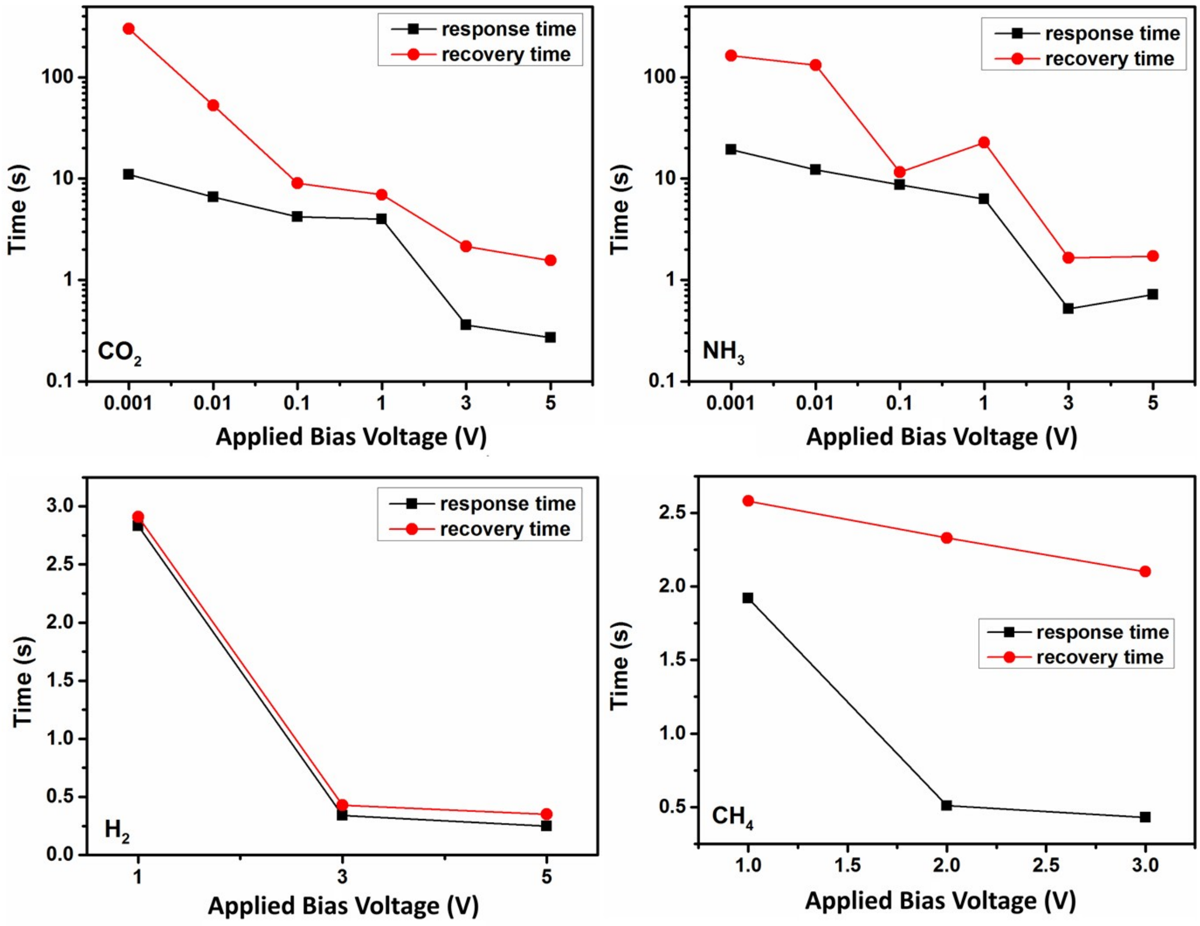

Figure S7. Calculated response and recovery times versus applied bias voltages of the Aerographite based sensor structures for: (a) CO_2; (b) NH_3; (c) H_2; and (d) CH_4 gases.

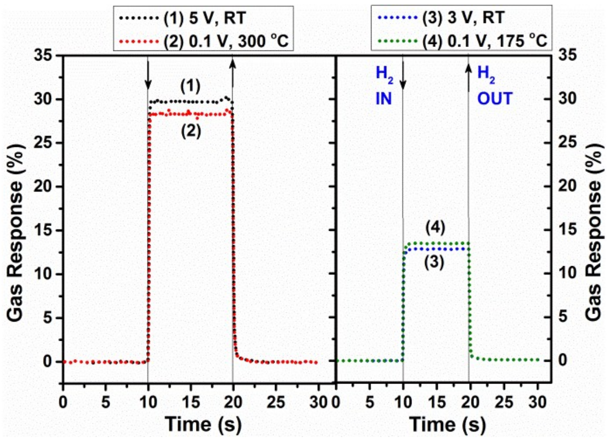

Figure S8. Dynamic gas response of interconnected graphitic tetrapods - Aerographite based sensor to 10 000 ppm H_2 gas: curve (1) at room temperature and 5 V applied bias voltage; curve (2) at 300 °C operating temperature and 0.1 V applied bias voltage; curve (3) at room temperature and 3 V applied bias voltage and curve (4) at 175 °C operating temperature and 0.1 V applied bias voltage.

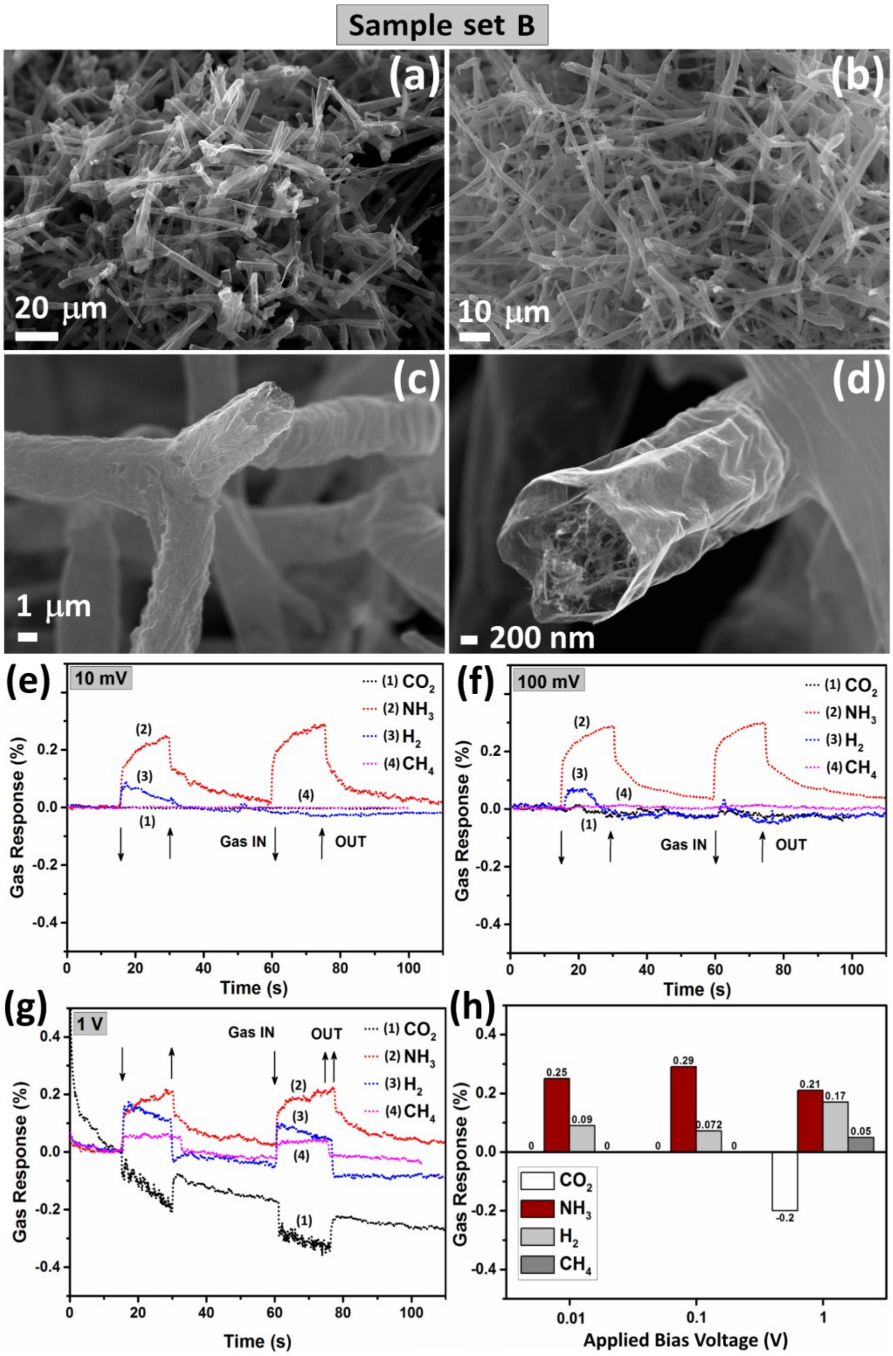

Figure S9. SEM images of Aerographite Sample set *B*: (a) overall view of graphitic tubular tetrapod network; (b) zoomed view of graphitic tubular tetrapod network; (c) a single graphitic tubular tetrapod with opened and closed ends; (d) nanographite tetrapod arms. Dynamic gas response of sensor structures based on Sample set *B* at room temperature for applied bias voltage of: (e) 10 mV; (f) 100 mV; and (g) 1 V. (h) Gas response versus applied bias voltage of Aerographite Sample set *B* based sensor structure.

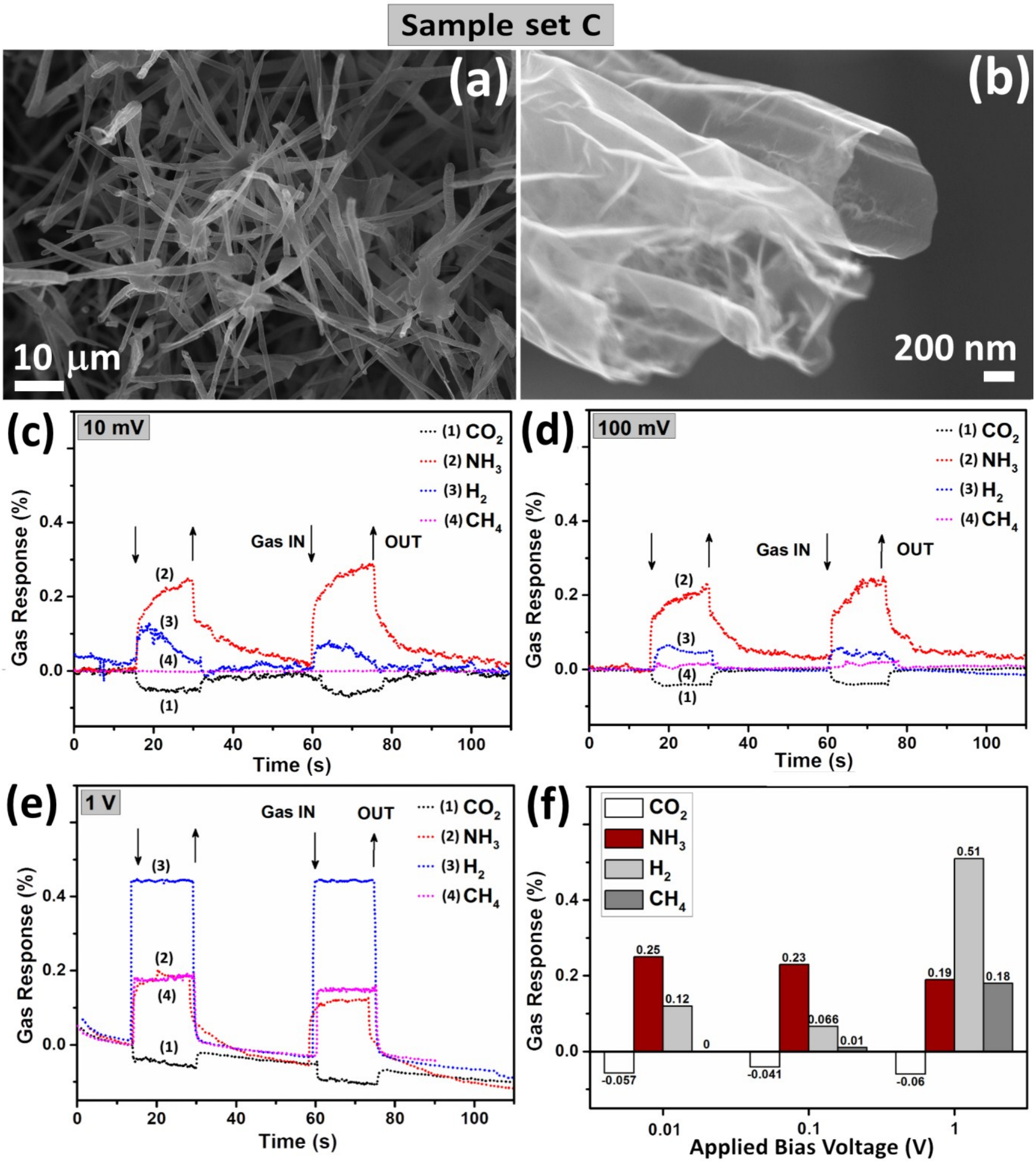

Figure S10. SEM images of Aerographite Sample set C: (a) overall view of graphitic tubular tetrapod network; (b) zoomed view of nanographite tetrapod arms. Dynamic gas response of sensor structures based on Sample set *C* at room temperature for applied bias voltage of: (c) 10 mV; (d) 100 mV; and (e) 1 V. (h) Gas response versus applied bias voltage of Aerographite Sample set *C* based sensor structure.

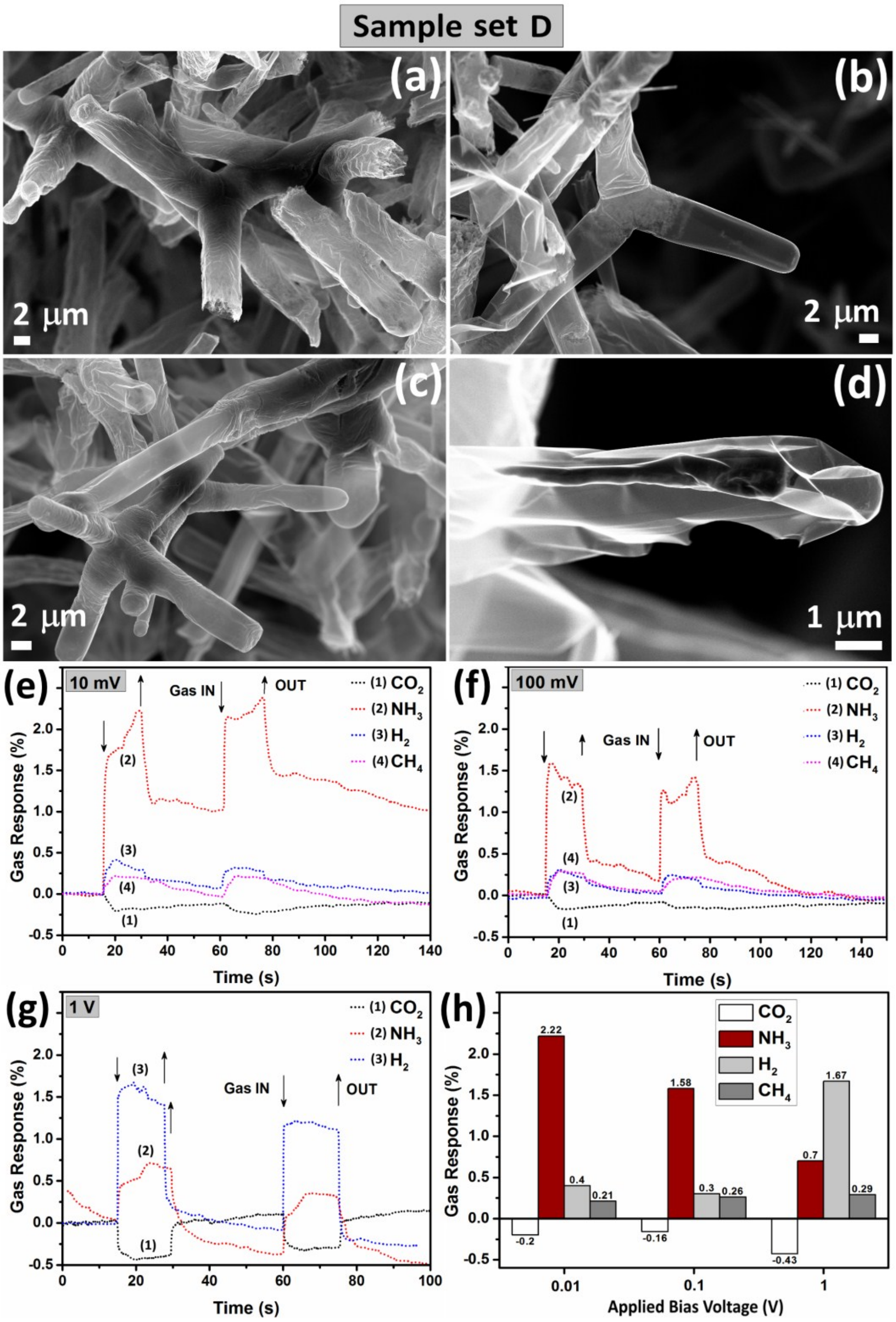

Figure S11. SEM images of Aerographite Sample set *D*: (a) overall view of graphitic tubular tetrapod network; (b-c) zoomed view of graphitic tubular tetrapod network; (d) a single graphitic tubular tetrapod with closed ends and ZnO residues inside it. Dynamic gas response of sensor structures based on Sample set *D* at room temperature for applied bias voltage: (e) 10 mV; (f) 100 mV; and (g) 1 V. (h) Gas response versus applied bias voltage of Aerographite Sample set *D* based sensor structure.

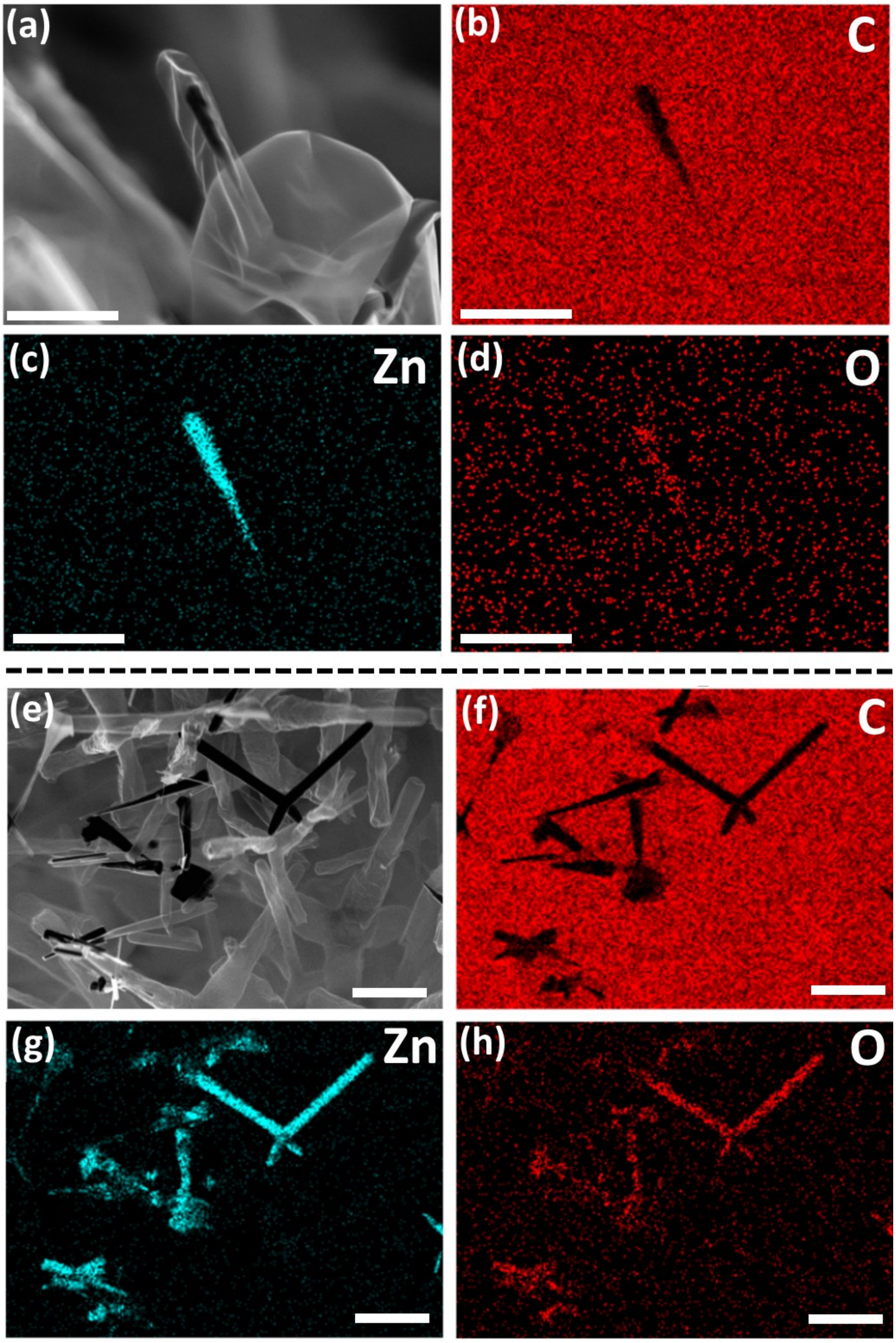

Figure S12. Compositional images taken by EDX elemental mapping at the microstructural level of Aerographite Sample set *B* (a-d) and set *D* (e-h) from two different regions: (a,e) SEM image of the studied regions; (b,f) C; (c,g) Zn and (d,h) O, respectively. The scale bar is 10 μm for (a-d) and 5 μm for (e-h), respectively.

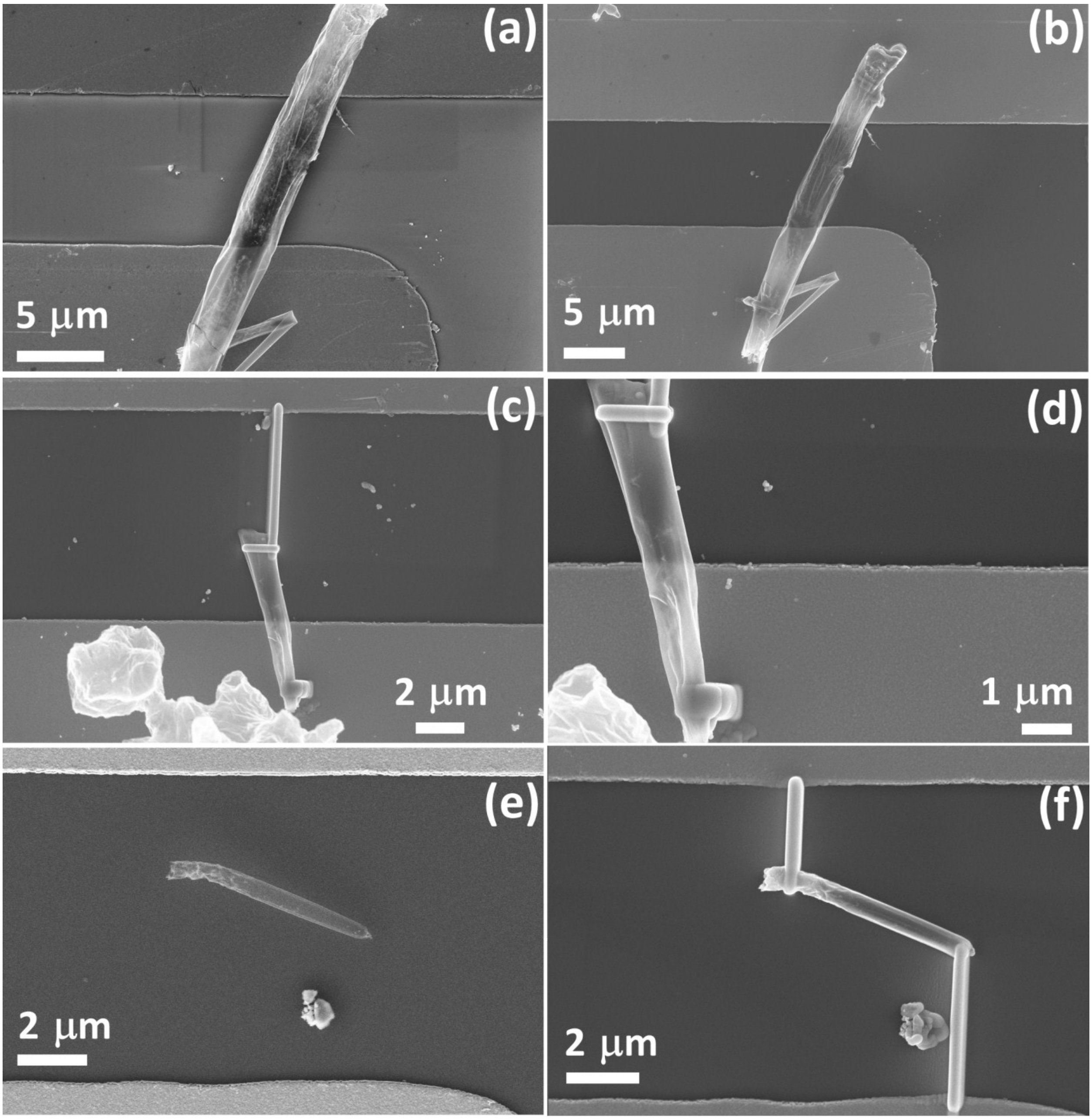

Figure S13. Functional devices based on a single graphene/nanographite tetrapod arm called Aerographite tubular microstructure. SEM images of the fabricated microsize devices based on tubular graphitic microstructures from Sample set *A* connected with Pt-complex to pre-patterned Au-pads chips in FIB-SEM: (a,b) D1, (c,d) D2 and (e,f) D3 configurations.

All devices were made using the procedure reported by Lupan et al.[1-8]

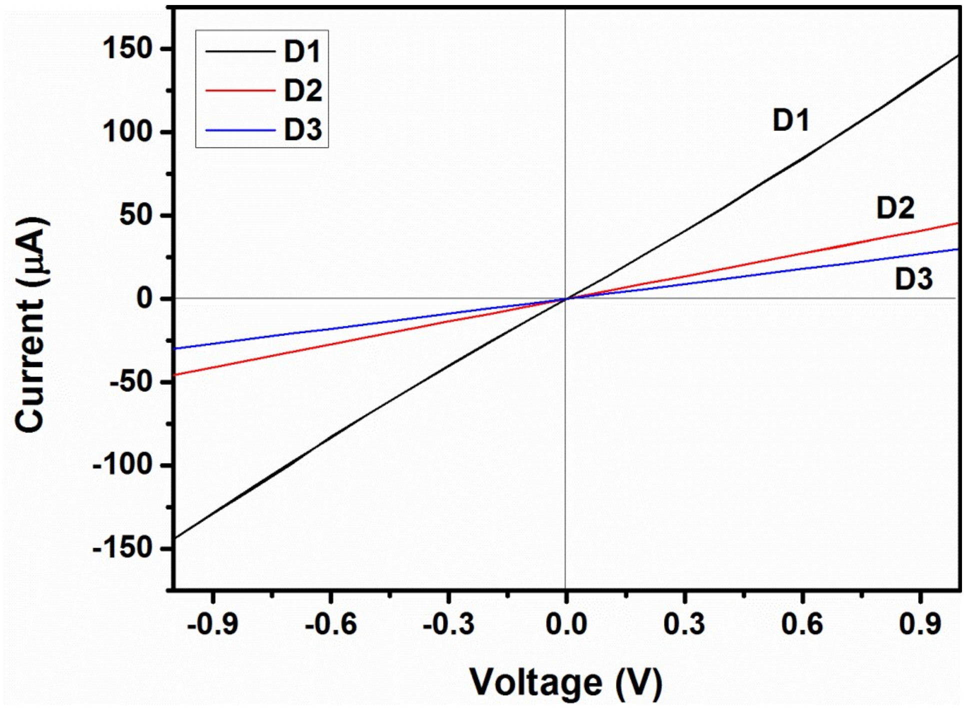

Figure S14. (a) Current – voltage characteristics of the sensor structures based on a single tubular graphitic microstructures at room-temperature RT.

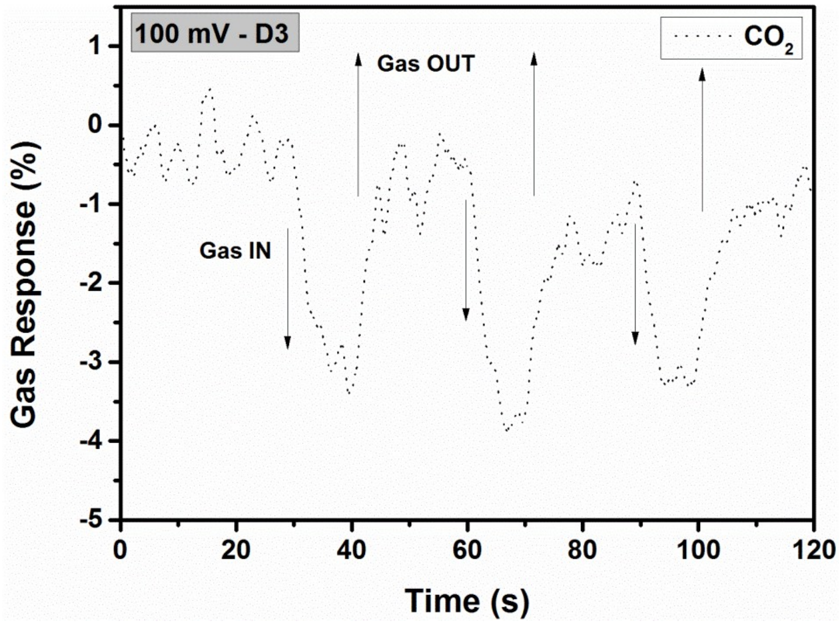

Figure S15. Dynamic CO_2 gas response at room temperature for applied bias voltage 100 mV to device D3 on a single tubular graphitic microstructure (microsensor).

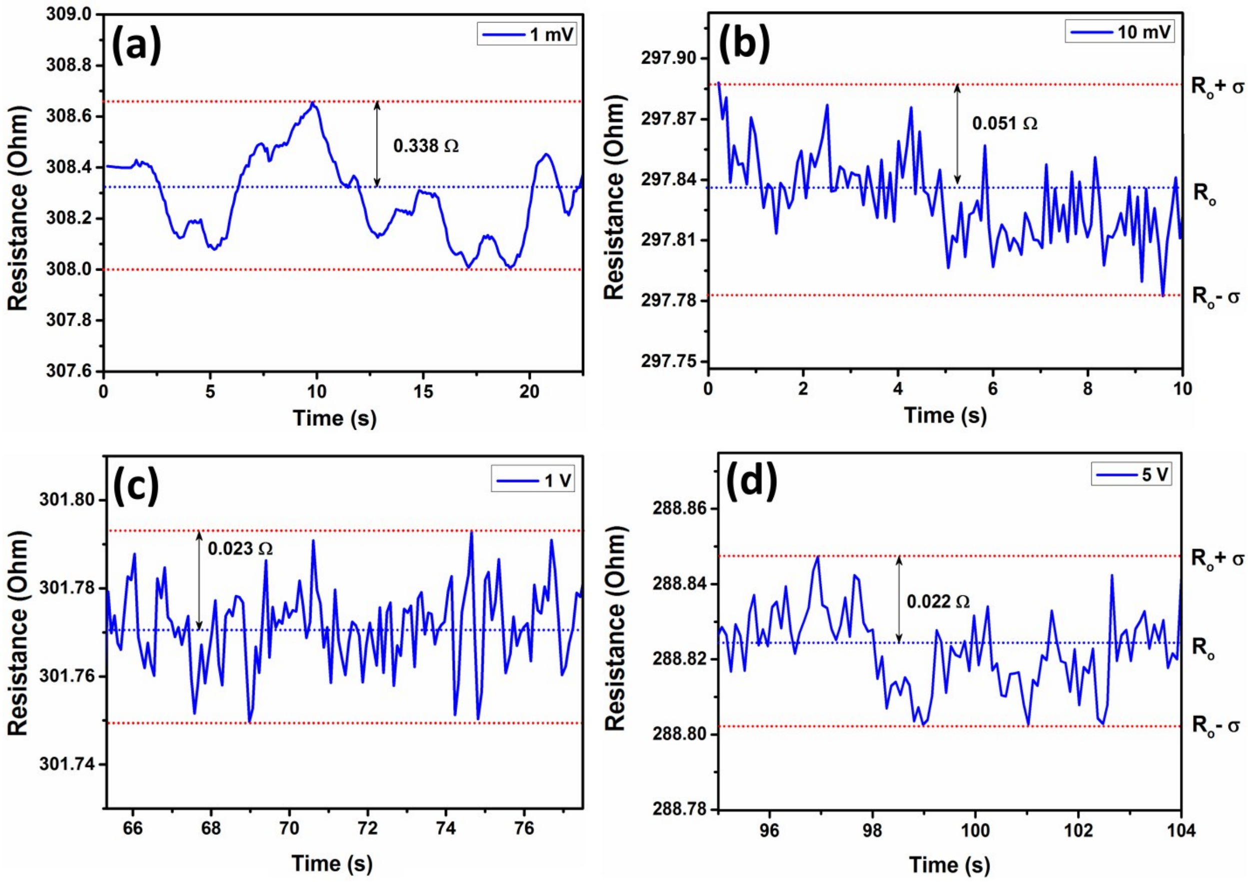

Figure S16. Determination of the standard deviation of the electrical signal before exposure to testing gas (σ) for applied bias: (a) 1 mV, (b) 10 mV, (c) 1 V and (d) 5 V (R_o is the resistance of sensor structure before exposure to test gas and it is the same as R_{air}).

Table S1. Parameters of Aerographite Sample set *A* based sensor structures

Applied bias (V)	Current value	Power consumption in air (mW)	Type of gas and conc. (ppm)	Gas response (%)	Operating temperature	Response Time (s)	Recovery time (s)	Signal to noise ratio (SNR)
0.001	≈ 3.6 µA	**≈ 3.6 nW**	CO_2, (500) NH_3, (100) H_2, (10 000) CH_4, (10 000)	- 0.53 0.71 - -	RT	11 19.33 - -	302 164 -	6.7 6.5 - -
0.01	36 µA	**≈ 360 nW**	CO_2, (500) NH_3, (100) H_2, (10 000) CH_4, (10 000)	- 0.57 1.05 - -	RT	6.6 12.2 - -	53 132 - -	29 21 - -
0.1	0.35 mA	**35 µW**	CO_2, (500) NH_3, (100) H_2, (10 000) CH_4, (10 000)	- 0.72 1.21 - -	RT	4.2 8.7 - -	9.02 11.58 - -	38 26 - -
1	3.3 mA	3.3 mW	CO_2, (500) NH_3, (100) H_2, (10 000) CH_4, (10 000)	- 3.83 1.78 1.58 0.87	RT	3.98 6.28 2.83 1.92	6.92 22.66 2.91 2.58	41 29 23 18
3	10.3 mA	30.9 mW	CO_2, (500) NH_3, (100) H_2, (10 000) CH_4, (10 000)	- 3.09 2.38 13.22 3.51	RT	0.36 0.52 0.34 0.51	2.15 1.65 0.43 2.33	46 36 236 51
5	17.6 mA	88 mW	CO_2, (500) NH_3, (100) H_2, (10 000) CH_4, (10 000)	- 5.37 4.45 31.84 7.6	RT	0.27 0.72 0.25 0.43	1.56 1.72 0.35 2.1	88 50 404 164

The signal to noise ratio (SNR) was defined as $|\Delta R|/\sigma$, where $|\Delta R| = |R_{gas} - R_{air}|$ and σ is the standard deviation of the electrical signal before exposure to testing gas (see Fig. S16).[9] Such relatively high SNR of Aerographite at applied bias voltages in range of 100 mV – 5 V was also reported by other authors for carbon based materials.[9, 10]According to the IUPAC definition, the signal is considered to be true if the SNR > 3,[11] thus we can consider that even at 1 mV applied bias the signal of sensor structure is a true signal.

Table S2. Geometrical and electrical parameters of the devices based on a single tubular graphitic microstructure.

Sensor device	Diameter of tube	Length total	Contact 1	Contact 2	Calculated resistance (Ohm)
D1	≈2.8 µm	≈ 28 µm	Au pad	Au pad	7531
D2	≈ 1 µm	≈ 7.7 µm	Pt/Au	Au pad	22098
D3	≈ 600 nm	≈ 6 µm	Pt/Au	Pt/Au	33543

More information about Aerographite materials can be found in our previous works[12-14].

References

1. O. Lupan, G. Chai and L. Chow, *Microelectron. J.*, 2007, **38**, 1211-1216.
2. O. Lupan, G. Chai and L. Chow, *Microelectron. Eng.*, 2008, **85**, 2220-2225.
3. O. Lupan, L. Chow and G. Chai, *Sens. Actuators B*, 2009, **141**, 511-517.
4. O. Lupan, V. Cretu, V. Postica, M. Ahmadi, B. R. Cuenya, L. Chow, I. Tiginyanu, B. Viana, T. Pauporté and R. Adelung, *Sens. Actuators B*, 2016, **223**, 893-903.
5. T. Pauporté, O. Lupan, J. Zhang, T. Tugsuz, I. Ciofini, F. d. r. Labat and B. Viana, *ACS Appl. Mater. Interfaces*, 2015, **7**, 11871-11880.
6. O. Lupan, V. V. Ursaki, G. Chai, L. Chow, G. A. Emelchenko, I. M. Tiginyanu, A. N. Gruzintsev and A. N. Redkin, *Sens. Actuators B*, 2010, **144**, 56-66.
7. O. Lupan, V. Postica, V. Cretu, N. Wolff, V. Duppel, L. Kienle and R. Adelung, *Phys. Status Solidi RRL*, 2015, **10**, 260-266.
8. I. Hölken, G. Neubüser, V. Postica, L. Bumke, O. Lupan, M. Baum, Y. K. Mishra, L. Kienle and R. Adelung, *ACS Appl. Mater. Interfaces*, 2016, **8**, 20491-20498.
9. F. Rigoni, S. Tognolini, P. Borghetti, G. Drera, S. Pagliara, A. Goldoni and L. Sangaletti, *Analyst*, 2013, **138**, 7392-7399.
10. J. Li, Y. Lu, Q. Ye, M. Cinke, J. Han and M. Meyyappan, *Nano Lett.*, 2003, **3**, 929-933.
11. L. A. Currie, *Pure Appl. Chem.*, 1995, **67**, 1699-1723.
12. S. Chandrasekaran, W. V. Liebig, M. Mecklenburg, B. Fiedler, D. Smazna, R. Adelung and K. Schulte, *Compos. Sci. Technol.*, 2016, **122**, 50-58.
13. M. Mecklenburg, A. Schuchardt, Y. K. Mishra, S. Kaps, R. Adelung, A. Lotnyk, L. Kienle and K. Schulte, *Adv. Mater.*, 2012, **24**, 3486-3490.
14. A. Schuchardt, T. Braniste, Y. K. Mishra, M. Deng, M. Mecklenburg, M. A. Stevens-Kalceff, S. Raevschi, K. Schulte, L. Kienle and R. Adelung, *Sci. Rep.*, 2015, **5**.